A Position and Speed Controller Tuning Method of Permanent Magnet Synchronous Linear Motor Based on Gain Identification

Yiwei Zhang, Xuzhen Huang, *Member, IEEE*, Anpeng Wang, and Jian Xu

***Abstract*—For permanent magnet synchronous linear motor (PMSLM), the traditional controller tuning method needs to identify the thrust coefficient and the mover mass separately. In order to simplify the parameter identification required for controller tuning of PMSLM, a strategy identifying the parameter named gain is proposed in this article. The gain is a parameter that combines the mover mass and thrust coefficient of PMSLM. The convergence time of the strategy is analyzed as well as the influence of the detent force on the identification error is investigated. After that, a controller tuning method based on the frequency domain is proposed and the geometric constraint relationship between the controller parameters is revealed. Eventually, combining the methods mentioned above, the experiment is carried out on a PMSLM prototype. The effectiveness of the proposed strategies is proved.**

***Index Terms*—Controller tuning, detent force, first-order filter, online gain identification, permanent magnet synchronous linear motor (PMSLM).**

I. Introduction

IN RECENT years, universal servo drives for permanent magnet synchronous linear motors (PMSLMs) have received more and more attention. As universal servo drives, it is required to be able to control motors with different parameters under changing conditions with excellent performance. Obviously, the parameters of motors, such as the mover mass and thrust coefficient, are of great significance for the controller to achieve superior dynamic and steady-state performance [1], [2]. For this reason, numbers of identification algorithms have been developed.

The mathematical models of the rotary and linear motors are similar. In addition, the literature on the rotary motors is abundant. The review will focus on rotary motors. The mover mass and thrust coefficient of linear motors are similar to the inertia and torque coefficient of rotary motors, respectively.

Manuscript received November 23, 2021; revised March 16, 2022; accepted May 8, 2022. Date of publication May 11, 2022; date of current version June 24, 2022. This work was supported by the National Natural Science Foundation of China under Grant 52022040. Recommended for publication by Associate Editor H. Hofmann. *(Corresponding author: Xuzhen Huang.)*

Yiwei Zhang and Xuzhen Huang are with the Department of Electrical Engineering, Nanjing University of Aeronautics and Astronautics, Nanjing 210016, China (e-mail: zywnuaa@126.com; huangxuzhen@nuaa.edu.cn).

Jian Xu is with the Wuxi Research Institute, Nanjing University of Aeronautics and Astronautics, Wuxi 214100, China (e-mail: jeansxu@163.com).

Anpeng Wang is with the Department of Electric Engineering, Harbin Institute of Technology, Harbin 150001, China (e-mail: hitwap@163.com).

Color versions of one or more figures in this article are available at https://doi.org/10.1109/TPEL.2022.3174417.

Digital Object Identifier 10.1109/TPEL.2022.3174417

Existing methods related to the moment of inertia identification can be categorized into three major groups: periodic speed commands method [3], [4], varying speed method [5]–[14], and harmonic injection method [15]. The periodic speed commands method can eliminate the influence of the viscous friction coefficient so as to improve identification accuracy. However, the load torque is considered unchanged in an identification cycle and the demand for periodic speed commands limits its application scenarios. The varying speed method usually has a closed-loop structure for which the periodic speed command is no longer needed. Therefore, its application scenarios are broader than that of the periodic speed command method. It mainly include observers [5]–[7], extended Kalman filter (EKF) [8]–[10], model reference adaptive system (MRAS) [11], [12], and recursive least squares (RLS) [13], [14]. However, lots of computational power is required and the viscous friction coefficient is ignored for these methods. The harmonic injection method is easy to be implemented and the influence of the viscous friction coefficient is taken into account. However, in offline identification, the load torque needs to be set to zero [15], which is difficult to be satisfied, whereas in online identification, the injected harmonic will affect the motor control performance.

For torque coefficient identification, there are three methods: direct measuring, offline testing, and online identification. The direct measuring method needs a force sensor and an experimental platform. Although it can be measured accurately, the cost is higher. The offline testing method is to test the inductance by measuring equipment [16] or high-frequency signal injected [1], [17], [18]. The permanent magnet flux can be calculated by no-load back electromotive force. In this way, the cost of the measurement can be reduced. The online identification method depends on the complex modern control theory, such as EKF [19], [20], MRAS [21], [22], RLS [23], and so on. A large number of scholars have carried out research on these methods and got great results. In [23], an identification method that depends on RLS is developed. The inductance and flux linkage can be identified separately. In account of the inverter nonlinearity, the results are accurate. However, this method is based on the steady-state voltage equation, which limits its feasible range.

In order to use the identified parameters, it is also necessary to study the controller parameter tuning strategy. The control system studied in this article adopts the three-closed-loop control structure, which is widely used in the industrial servo field.

Since the position controller is a proportional controller and the speed controller is a proportional–integral controller, there are mainly three kinds of tuning methods: pole–zero method [24], frequency-domain method [25]–[28], and the principle of internal model [29], [30]. The pole–zero method affects the performance of the control system by changing the position of the pole in the controller. Less amounts of computation are needed in this method. However, it only qualitatively describes the performance of the control system. For the frequency-domain method, the performance of the control system can be calculated quantitatively by designing the bandwidth and phase margin, although the calculation amount is larger than those of others. In [29], the tuning process has been simplified by designing an internal model controller, but there is still one parameter that needs to be tuned.

In summary, it is very complicated to identify the torque coefficient and the moment of inertia separately for controller designing. This article proposes to combine the torque coefficient and the moment of inertia into one parameter, named gain. It is a ratio of K_f to M (K_f is the thrust coefficient and M is the mover mass). To eliminate the influence of viscous friction coefficient during identification, periodic speed commands, such as sinusoidal, triangular, and trapezoidal waveforms, are given as the reference to the speed controller. Moreover, low-pass filters are added to eliminate the sampling noise. The proposed gain identification method can be used both offline and online.

In offline identification, the sinusoidal waveform is given for its better precision, and the identification results are used for controller design. In online identification, the PMSLM is reciprocating in position mode. The periodic reciprocating movement increases the value of algorithm applications. The position controller will output the triangular or trapezoidal waveform to the speed controller as a reference by which the servo driver can accomplish adaptive controller parameter adjustment.

A position and speed controller design method based on the gain is proposed. On the basis of the article presented in [27], the geometric constraint relationship between the proportional coefficient and the integral coefficient has been further derived in this article. Eventually, the proposed method is implemented in the microcontroller.

The experiments are carried out on a PMSLM, and the effectiveness of the proposed strategy has been proved.

II. Mathematical Model of PMSLM

Due to the adoption of a vector control strategy with $i_d = 0$, the motion equation of PMSLM can be described as

$$\begin{cases} F_e = Bv + M\dot{v} + F_d + F_f \\ F_e = K_f i_q \end{cases} \tag{1}$$

where F_e is the electromagnetic thrust; i_q is the q-axis current; B is the viscous friction coefficient; v is the speed of mover; $\dot{v}$ is the differential of speed; and F_d is the detent force and F_f is the friction of the slide.

The traditional transfer function model of the speed loop is shown in Fig. 1(a) in which M and K_f are needed to tune the controllers. As what has been mentioned in Section I, it is complicated to identify these two parameters separately. Since the relationship between the input and output should be paid more attention, the M can be put in the front position, so K_f and M can be combined into one parameter, as shown in Fig. 1(b). In this model, the controller can be designed as usual and the identifying process can be simplified.

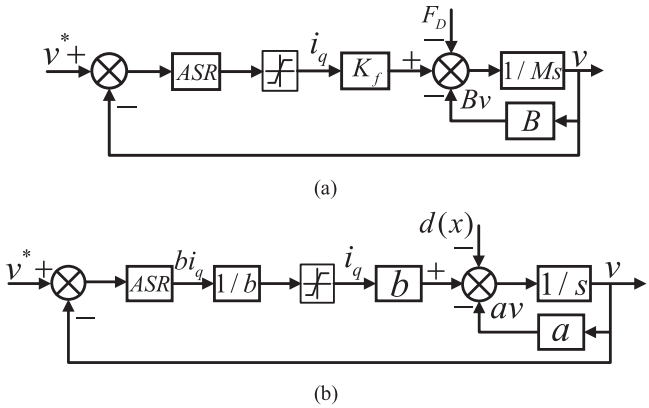

Fig. 1. Gained speed loop frequency-domain model. (a) Traditional transfer function model. (b) Transfer function model of the speed loop in gain form.

The motion equation of PMSLM can be transformed as

$$bi_q = av + \dot{v} + d(x) \tag{2}$$

where b is the gain; a is the $\frac{B}{M}$; b is the $\frac{K_f}{M}$; $d(x)$ is the $\frac{F_D}{M}$, and F_D is the disturbance thrust, including friction and detent force.

Since the viscous friction coefficient is usually small, a does not need to be identified. The parameters M and K_f are combined into one. It can simplify the identification process.

III. Proposed Gain Identification Strategy

In this section, a gain identification strategy is developed with consideration of the sampling noise and disturbance thrust. The relationship between the cutoff frequency and the convergence time of the identification strategy after adding the low-pass filter is derived. The cutoff frequency of the filter is designed considering both the convergence time and identification error.

A. Derivation of the Identification Strategy

It is assumed that the parameters K_f, B, and F_f remain unchanged during the identification period. At the start of the identification, the initial value of M is set to $M(0)$, so the identification equation of gain can be constructed as

$$x(0) = K_f i_q - M(0)\dot{v} = \Delta M\dot{v} + Bv + F_D \tag{3}$$

where $x(0)$ is the estimation of M, and $\Delta M = M - M(0)$.

If the speed command is a symmetrical signal with a period of T, such as sinusoidal, trapezoidal, triangle, and so on, the speed and its derivative in a period satisfies the following relationship:

$$\begin{cases} \sum_{t=0}^{T} v = 0 \\ \sum_{t=0}^{T} \dot{v} = 0 \\ \sum_{t=0}^{T} v \times \dot{v} = 0 \end{cases} \tag{4}$$

where T is the period of the speed command and t is the time.

According to the relationship between the speed and its differential, and multiply $\dot{v}(t)$ around (3), the following equation can be obtained:

$$\sum_{t=0}^{T}\{[K_f i_q(t) - M(0)\dot{\hat{v}}(t)]\times \dot{\hat{v}}(t)\} = \Delta M \sum_{t=0}^{T} \dot{\hat{v}}^2(t) + \sum_{t=0}^{T} \dot{\hat{v}}(t) F_d. \tag{5}$$

Combing (4) and (5), M can be calculated by

$$M = \frac{K_f \sum_{t=0}^{T} i_q(t)\dot{\hat{v}}(t) - \sum_{t=0}^{T} \dot{\hat{v}}(t) F_d}{\sum_{t=0}^{T} \dot{\hat{v}}^2(t)}. \tag{6}$$

Obviously, the parameter gain can be derived from (6).

$$b = \frac{\sum_{t=0}^{T} \dot{\hat{v}}^2(t)}{\sum_{t=0}^{T} i_q(t)\dot{\hat{v}}(t) - \frac{1}{K_f}\sum_{t=0}^{T} \dot{\hat{v}}(t) F_d}. \tag{7}$$

B. Design of the Low-Pass Filter

A low-pass filter is studied to eliminate the noise. If the speed and current are processed by the same first-order low-pass filter, such as $\lambda/(S+\lambda)$, the following formula can be obtained:

$$K_f q_3 = B q_2 + M q_2 s + F_D q_1 \tag{8}$$

where q_1, $q_2(t)$, and $q_3(t)$ are the transfer functions of the low-pass filter, filtered speed, and filtered current, respectively.

From (8), the friction is not a constant anymore before converging. Thus, the convergence time of identification is equal to that of friction.

Combing (6) and (8), the gain can be further derived as

$$b = \frac{\sum_{t=0}^{T} \dot{q}_2^2(t)}{\sum_{t=0}^{T} \dot{q}_2(t) q_3(t) - \frac{1}{K_f}\sum_{t=0}^{T} \dot{q}_2(t) q_1 F_d}. \tag{9}$$

Since the value of $\frac{1}{K_f}\sum_{t=0}^{T} q_2(t) q_1 F_d$ cannot be measured, this item should be ignored. Therefore, it is the source of the identification error. Combining the transfer function of the low-pass filter and the detent force, the following formula can be obtained:

$$\delta_n = \frac{1}{K_f}\sum_{t=0}^{T} \dot{q}_2(t) q_4(t) \tag{10}$$

where $q_4(t)$ is the product of the function of detent force and low-pass filter, and δ_n is the identification error.

The block diagram of gain identification can be shown in Fig. 2.

Since the detent force is composed of a series of harmonics [31], the lower the cutoff frequency of the low-pass filter, the smaller the identification error. However, the identification convergence time depends on the cutoff frequency. The lower the cutoff frequency, the longer the convergence time. Therefore, a compromise must be made between the convergence time and the identification error. The rise time of the step response of the first-order low-pass filter is as

$$t_s = -\frac{\ln(0.01)}{\lambda} \tag{11}$$

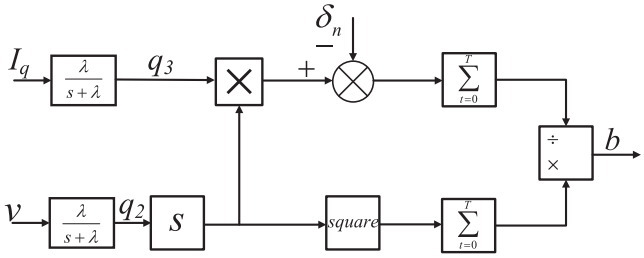

Fig. 2. Block diagram of the gain identification.

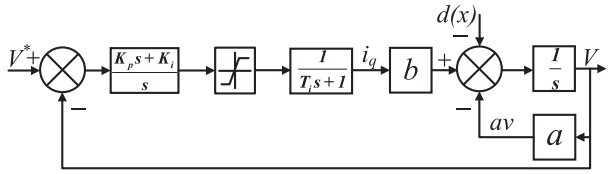

Fig. 3. Block diagram of the speed loop frequency-domain model.

where λ and t_s are the cutoff frequency and rise time, respectively.

Combining the identification period and (11), the identification convergence time is calculated by

$$t_r = \left[\text{ceil}\left(\frac{t_s}{T}\right) + 1\right] \times T \tag{12}$$

where t_r is the identification convergence time; and ceil() is the round-up function.

In order to ensure that the mover speed is not too fast to cause vibration, the identification period is set to 0.4 s. Thus, the cycle of the identification is 1.2 s. To ensure that the gain can converge within one cycle and the cutoff frequency is low enough to eliminate the identification error, the cutoff frequency is selected as 6 rad/s. The low-pass filter can eliminate the influence of the detent force, and the formula of gain identification can be obtained eventually by

$$b = \frac{\sum_{t=0}^{T} \dot{q}_2^2(t)}{\sum_{t=0}^{T} \dot{q}_2(t) q_3(t)}. \tag{13}$$

IV. Proposed Position and Speed Controller Tuning Method

A position and speed controller tuning method based on the frequency domain is developed in this section. This method considers the geometric constraint relationship between the proportional coefficient and the integral coefficient. Besides, its implementation method in the microcontroller is given.

A. Derivation of the Tuning Method

Since the control period of the speed loop is ten times the current loop, the current loop can be simplified as a first-order inertia link during the tuning of the speed and position loop. The diagram of the speed loop can be obtained, as shown in Fig. 3. K_p, K_i, s, and T_i are the proportional and integral coefficients

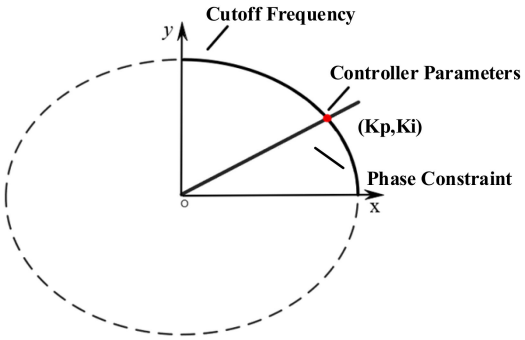

Fig. 4. Geometric relationship between K_p and K_i.

of the speed loop, the differential operator, and the current loop equivalent inertia coefficient, respectively. The open-loop transfer function of the speed loop can be obtained as

$$G_o(s) = \frac{K_p s + K_i}{T_i s^3 + (aT_i + 1)s^2 + as} \tag{14}$$

where $G_o(s)$ is the transfer function of the open speed loop.

From (14), a set of equations based on the open-loop cutoff frequency and phase margin can be further derived as

$$\begin{cases} \frac{\sqrt{{K_p}^2\omega_c{}^2 + {K_i}^2}}{\omega_c\sqrt{\left(1+{T_i}^2\omega_c{}^2\right)\sqrt{(\omega_c{}^2+a^2)}}} = 1 \Rightarrow \frac{{K_p}^2}{m^2} + \frac{{K_i}^2}{n^2} = 1 \\ \left(\arctan(\frac{K_p\omega_c}{K_i}) - \arctan(T_i\omega_c) - \arctan(\frac{\omega_c}{a})\right) + \frac{\pi}{2} = \varphi_m \\ \Rightarrow \frac{K_p}{K_i} = k \end{cases} \tag{15}$$

where ω_c, m, n, φ_m, and k are the open-loop cutoff frequency of the speed loop, the length of the major axis, the length of the minor axis, the phase margin, and the slope of the straight line, respectively.

From (15), the geometric relationship between K_p and K_i can be obtained as the intersection of the ellipse and the straight line in the first quadrant, as shown in Fig. 4.

Since the position controller is a proportional controller, the phase margin cannot be adjusted. Its open-loop cutoff frequency is usually set to one-tenth of that of the speed loop

$$\frac{K_{pp}}{\sqrt{(\omega_{cp}{}^2 + a^2)}} = 1 \tag{16}$$

where K_{pp} and ω_{cp} are the proportional coefficient and the open-loop cutoff frequency of the position loop, respectively.

B. Realization Method in the Microcontroller

Since the viscous coefficient is usually small enough to be negligible, the calculation formulae of K_p, K_i, and K_{pp} in the microcontroller are given as

$$\begin{cases} K_i = \frac{{\omega_c}^2}{b\sqrt{1+k^2}} \\ K_p = \frac{kK_i}{\omega_c} \\ K_{pp} = \frac{\omega_c}{10b} \end{cases} \tag{17}$$

where k is $\tan(\arctan(T_i\omega_c) + \varphi_m)$.

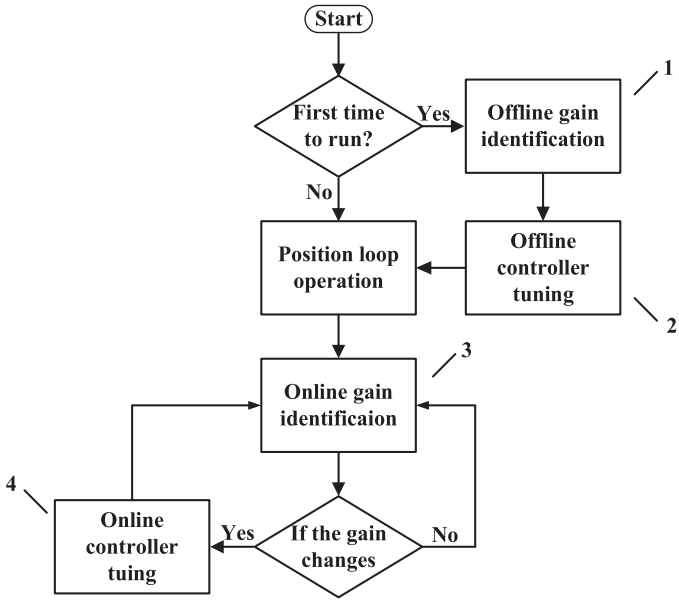

Fig. 5. Flowchart of the online and offline tuning methods.

Thus, the tuning method of the position and speed controllers in both offline and online conditions based on the gain identification can be obtained, as shown in Fig. 5.

The flowchart, as shown in Fig. 5, is divided into four steps as follows:

1) offline gain identification;
2) offline tuning;
3) online gain identification;
4) online tuning.

After a few periods of offline commissioning to identify the gain, the controllers can get great performance when startup. Then, the servo system can be put into use. However, the mass load of the system may change during the running, so the identification scheme should be implemented. In this way, the gain can be identified in real time and the controllers can be tuned to keep the performance of the system.

V. Experimental Results

The identified gain is used to tune the position and speed controllers in both offline and online conditions. The offline tuning can provide suitable controller parameters when the motor starts running, and the online tuning can update parameters according to load changes. The experiments were carried out on the platform, as shown in Fig. 6.

The cutoff frequency of the low-pass filter is chosen as 6 rad/s and the gain converged after three speed command periods. The controller parameters are shown in Table II.

The experimental control system is composed of STM32F407IG and Cyclone IV E EP4CE10F17C8 and the position sensor uses a magnetic scale with an accuracy of 0.5 microns per pulse. microcontroller unit (MCU) is responsible for algorithm realization, while field programmable gate array (FPGA) is used for position signal decoding, fault

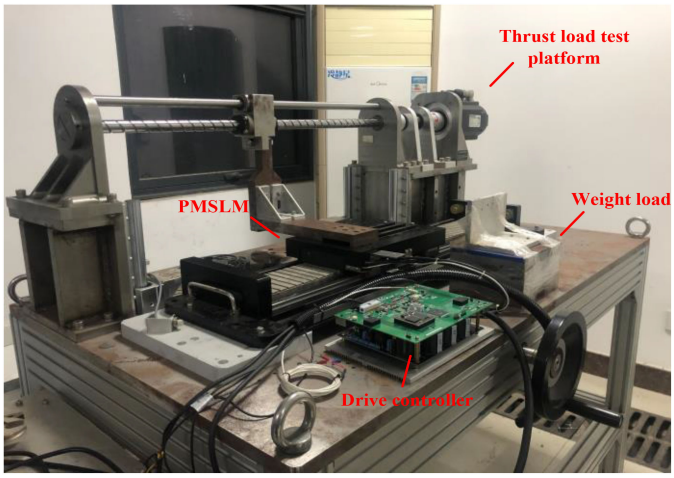

Fig. 6. PMSLM thrust and mass load test platform.

TABLE II
IDENTIFIED GAIN AND PARAMETERS OF CONTROLLER BEFORE AND AFTER IDENTIFICATION

Parameter	Offline Test	Online Test 1	Online Test 2	Online Test 3
No-load Gain	11.8	11.17	11.97	12.5
Load Gain	\	3.73	3.99	3.81
K_{ppb}	1	3.4	3.17	3.04
K_{pb}	17	35	32.7	31.3
K_{ib}	1300	3065	2860	2739
K_{ppa}	3.41	9.92	9.27	9.71
K_{pa}	34.8	102.1	95.45	100
K_{ia}	3091.8	9051	8461.2	8861

TABLE I
PARAMETERS OF THE PMSLM

Parameters	Value
Rated DC voltage	180 V
Rated Current	6 A
Rated mover velocity	1 m/s
Phase winding resistance	3.48 Ω
Phase winding self-inductance	38 mH
Thrust coefficient	137 N/A
No-load Gain	11.81N/A/Kg
Load Gain	4.04N/A/Kg
Mover mass	11.6 Kg
Load mass	22.3 Kg
Viscous friction coefficient	0.0076
Switching frequency	10 kHz
Control frequency of speed loop	1 kHz

protection, and control of digital-to-analog conversion chip. The data sampling is realized through J-scope, and the maximum sampling channel is 10. The parameters of the slotted PMSLM are listed in Table I.

A. Offline Controller Tuning Experiment

Three kinds of speed commands are given. In order to verify whether the gain can be converged accurately, the controllers are given a set of initial parameters with a low bandwidth to ensure that the motor will not oscillate under the condition of unknown gain.

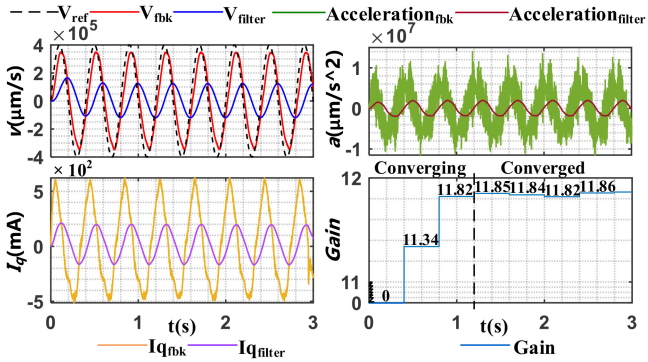

Fig. 7. Sinusoidal waveform speed command experimental waveform.

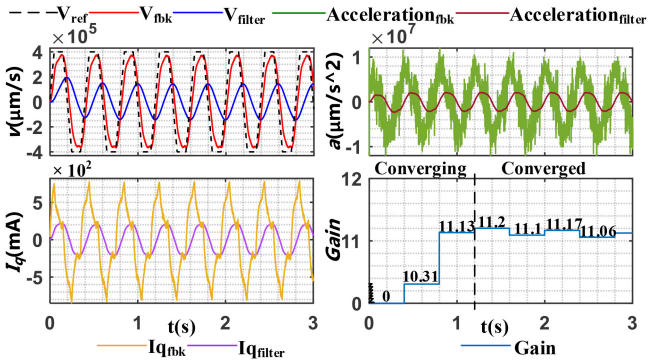

Fig. 8. Trapezoidal waveform speed command experimental waveform.

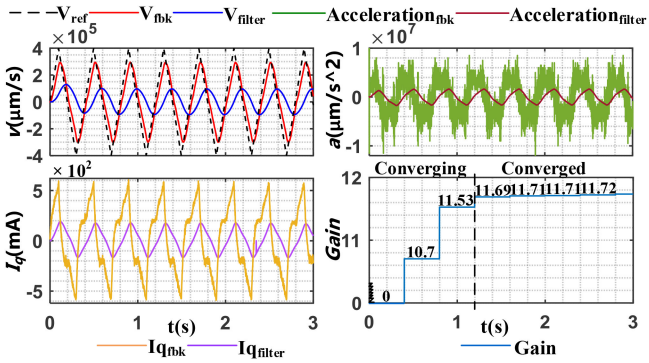

Fig. 9. Triangular waveform speed command experimental waveform.

When the sinusoidal waveform speed command is given, the feedback of mover velocity is compared with the reference in Fig. 7. Although the feedback lags the reference and the amplitude is reduced, it is still a symmetrical sinusoidal waveform. The gain can converge to 11.85 and the error is about 0.34%.

Then, the trapezoidal waveform speed command is given and the results are shown in Fig. 8. Due to the low control bandwidth, the feedback cannot fully track the reference and it is not a well-symmetrical waveform. The gain converges to 11.2 and the identification error is 5.17%.

Eventually, the triangular waveform speed command is given, and the experimental results are shown in Fig. 9. The symmetry of the feedback is better than that of a trapezoidal waveform, and

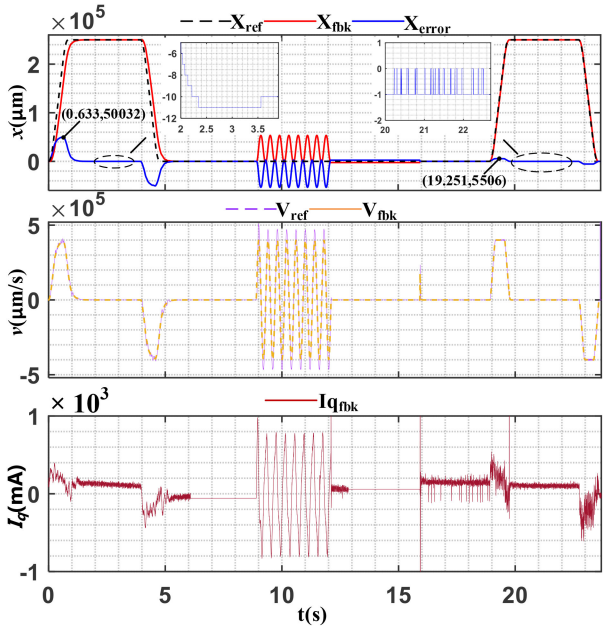

Fig. 10. Offline controller tuning experimental waveforms.

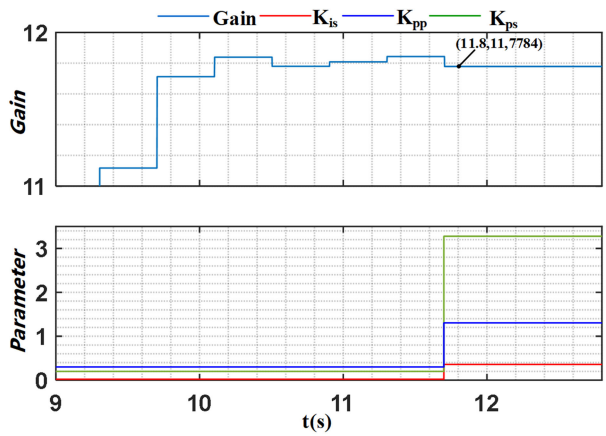

Fig. 11. Identified gain and tuned controller parameters of offline tuning.

the gain converges to 11.69 and the error is 1.02%. The above experiments show that the better the symmetry of the feedback speed waveform, the smaller the identification error.

It can be seen from Figs. 7–9 that, after filtering, the noise of the q-axis current and acceleration has been eliminated, thereby improving the accuracy of identification.

Moreover, (10) shows that detent force, which is a function of position, also causes the identification error. Thus, at different speeds, the error caused by the detent force will be different.

The identification error under the sinusoidal waveform speed command is the smallest because of the better symmetry. Thus, the sinusoidal waveform speed command is used to perform the tuning calculation in the offline controller tuning experiment.

The offline tuning experiments are divided into three stages: before tuning, gain identification, and after tuning.

In the first 6 s of the position loop, as shown in Fig. 10, under the initial control parameters, the maximum position tracking error is 50 032 μm, which shows that the dynamic performance of the controller is poor. In the steady-state stage, the positioning error is more than 10 microns, which shows that the ability of the controller to eliminate the steady-state error is also poor. Gain identification begins to run in the ninth second and a new set of the controller parameters is tuned. Then, run the motor in the position loop again. The maximum positioning error is reduced to 5506 μm. The steady-state error is less than 1 μm. It means that the parameter tuning strategy based on the gain identification extremely improves the position tracking performance of the controller. The offline test in Table II exhibits the gain, and the controller parameters before and after tuning. Among them, K_{ppb}, K_{pb}, and K_{ib} are the proportional coefficients of the position loop, and proportional and integral coefficients of the speed loop before tuning, respectively, while K_{ppa}, K_{pa}, and K_{ia} are the controller parameters after tuning.

From Fig. 11, the tuned controller parameters are calculated from the last identification result. Moreover, in the control system, the parameters are per unit (PU) value, while in Table II, they are named value.

B. Online Controller Tuning Experiment

Online controller tuning means that the motor performs the handling work in the position loop. To run the motor in constant acceleration, the position trajectory planner outputs the commands to the position controller by integrating the trapezoidal or the triangular waveform. Then, the position controller outputs a symmetrical speed command, which is similar to the triangular or the trapezoidal waveform. Thus, the online controller tuning can be performed.

First, an online tuning experiment based on the trapezoidal speed command under the initial parameters is carried out. The experiments are also designed, which are divided into three stages: before tuning, no-load tuning, and load tuning. The results are shown in Figs. 12 and 13.

In the first 5 s, under the initial parameters, due to the poor position tracking performance, the feedback speed waveform is not an idea trapezoidal waveform. However, due to its symmetry, the gain identification can still converge to the correct value. It can be seen that the gain has converged at about fifth second, then the three parameters of the controllers are linearly updated through the gain identification. Then, at the ninth second, the load is suddenly added to the mover. After three cycles, the gain is identified and the parameters of the controllers are linearly updated again. By comparing the position tracking waveforms before and after tuning, both the speed and position tracking have been greatly improved after tuning. The positioning errors are reduced to less than half of those before tuning and the feedback speed finally becomes a trapezoidal waveform. In the third stage, due to the increase of the mass, the anti-interference performance of the system is improved and the position tracking error is reduced. The online test 1 in Table II exhibits the gain and the controller parameters. The parameters in Table II are calculated

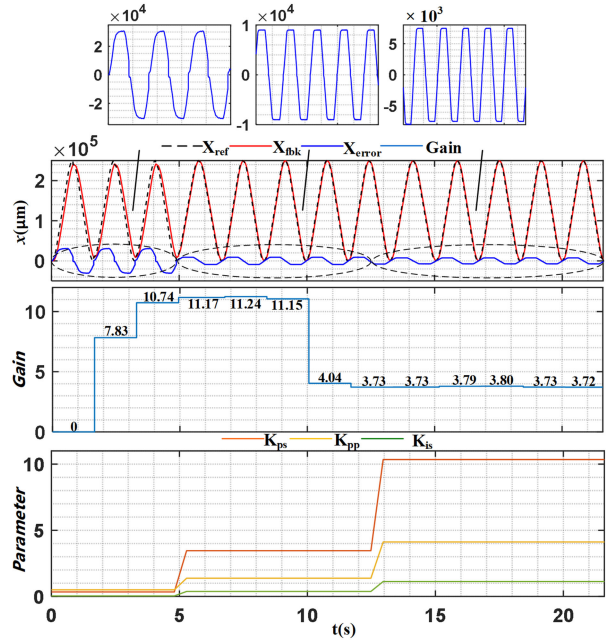

Fig. 12. Online controller tuning based on the trapezoidal waveform speed command experimental waveform.

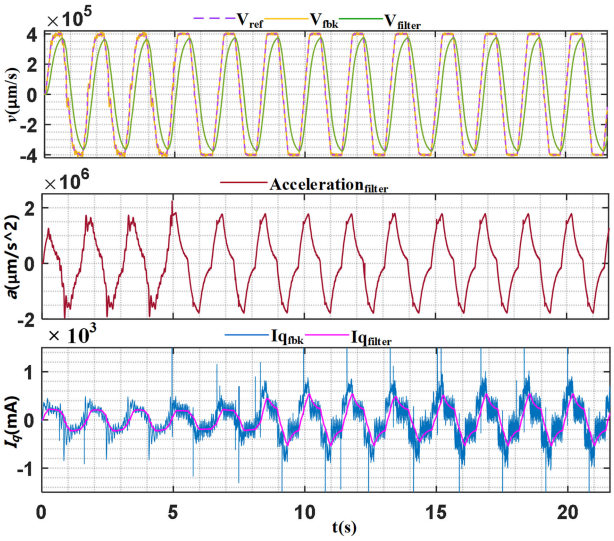

Fig. 13. Online controller tuning based on the trapezoidal waveform speed command experimental waveform.

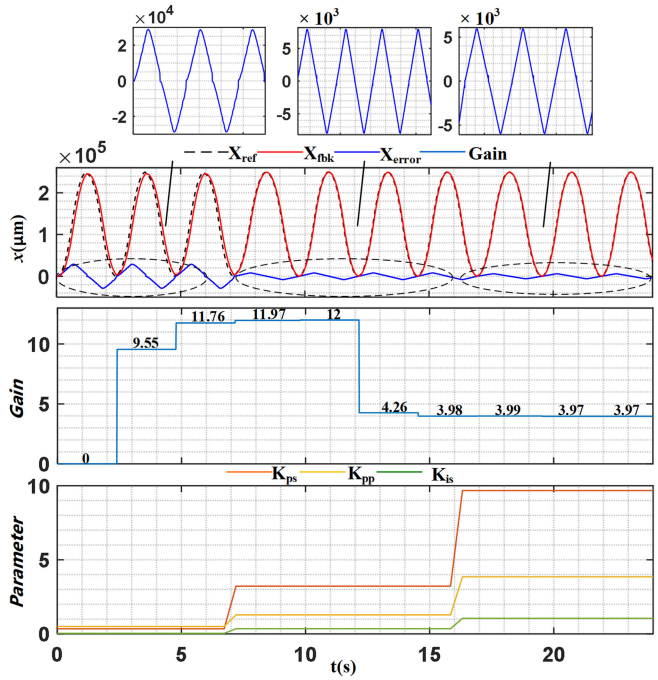

Fig. 14. Online controller tuning based on the triangular waveform speed command experimental waveform.

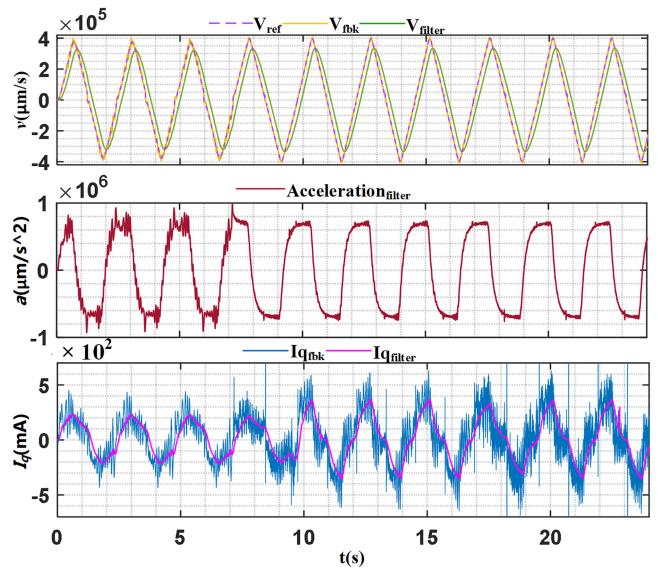

Fig. 15. Online controller tuning based on the triangular waveform speed command experimental waveform.

by the formula given in Section IV, while the parameters in Fig. 12 is the PU value of them.

Then, an online tuning experiment based on the triangular speed command under the initial controller parameters is carried out. The results are shown in Figs. 14 and 15.

Similarly, the experiment is also including the three stages. Due to the continuity of the triangular waveform, the feedback velocity still has good symmetry under the initial parameters. The controller parameters are linearly updated when the gain is converged at the 7th and 16th second. After controller tuning, the speed and position tracking performance and steady-state performance are greatly improved. The online test 2 in Table II exhibits the gain and the parameters.

Eventually, an online tuning experiment based on the sinusoidal speed command under the initial controller parameters is carried out for validation. The results are shown in Figs. 16 and 17.

Since the position reference has to change from zero, its velocity initially has a step. At this point, the acceleration will

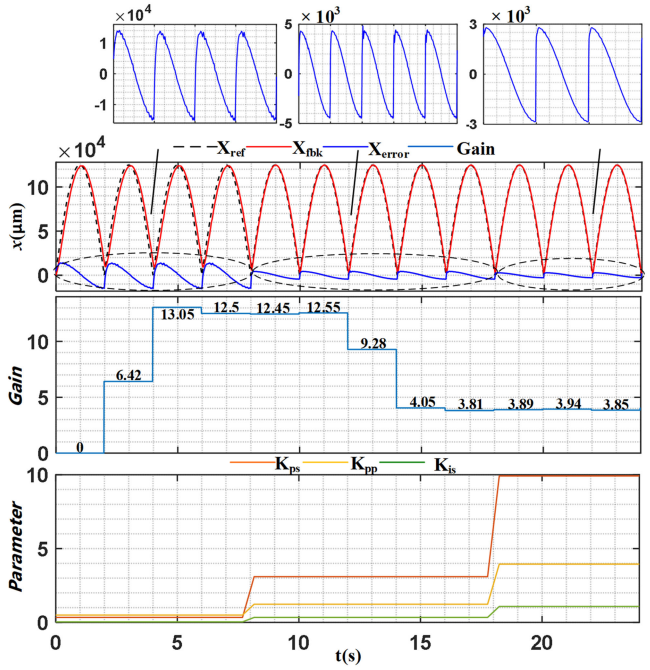

Fig. 16. Online controller tuning based on the sinusoidal waveform speed command experimental waveform.

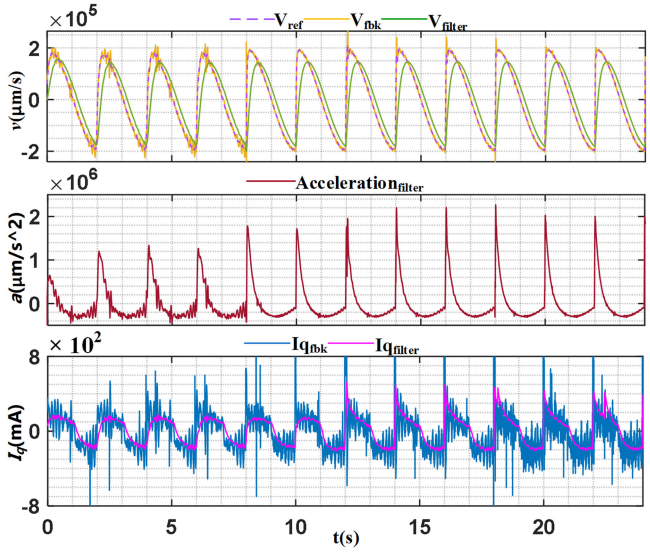

Fig. 17. Online controller tuning based on the sinusoidal waveform speed command experimental waveform.

reach the limit value, which may lead to a large overshoot and oscillation.

For the reason that the velocity is initially a step, its symmetry was affected; however, the gain can still converge.

After the controller parameters are updated linearly, the tracking performance and the steady-state performance of the velocity and position controllers are greatly improved.

Comparing the above three different velocity references, the sinusoidal reference is usually not used in position control because of the large and uncontrollable acceleration. Due to the poor tracking performance under the initial parameters, the trapezoidal reference has larger errors, while the triangular reference has the best identification performance among them.

VI. Conclusion

In this article, an identification strategy combining the mover mass and the thrust coefficient into a parameter named gain is proposed. A low-pass filter is designed to eliminate the noise of current and speed in identifying the gain. Moreover, a position and speed controller tuning method is studied. The offline and online experiments are carried out to demonstrate the effectiveness of the proposed scheme. In offline experiments, the gain converges in three cycles of speed command period and the position tracking performance is greatly improved. In online experiments, the gain converges when the mass load is suddenly added, and the position tracking performance can be maintained. These experiments prove that the proposed scheme can improve both the startup and running performances of the PMSLM in the position servo system. In addition, the research of this article is based on a PMSLM, whose characteristics and mathematical model are as same as the rotary permanent magnet synchronous motor (PMSM). Therefore, the proposed scheme can be implemented in rotary PMSM as well.

In the actual control process, although the steady-state error caused by friction can eventually be compensated by the integrator, it will affect the dynamic performance of the controller. Therefore, further research on method for synchronously identifying gain and friction is required in the future.

References

[1] Q. Wang, G. Zhang, G. Wang, C. Li, and D. Xu, "Offline parameter self-learning method for general-purpose PMSM drives with estimation error compensation," *IEEE Trans. Power Electron.*, vol. 34, no. 11, pp. 11103–11115, Nov. 2019.

[2] Z.-H. Liu, H.-L. Wei, X.-H. Li, K. Liu, and Q.-C. Zhong, "Global identification of electrical and mechanical parameters in PMSM drive based on dynamic self-learning PSO," *IEEE Trans. Power Electron.*, vol. 33, no. 12, pp. 10858–10871, Dec. 2018.

[3] K. Cho and K. Nam, "System identification method based on a disturbance observer using symmetric reference trajectories in PMLSM-based motion systems," *IEEE Access,* vol. 8, pp. 216197–216209, 2020.

[4] C. Wu, L. Zheng, and E. Zhi, "Mechanical parameter identification of permanent magnet servo systems based on orthogonality of trigonometric functions," in *Proc. CSEE*, 2022, pp. 1–9.

[5] C. Yang, B. Song, Y. Xie, and X. Tang, "Online parallel estimation of mechanical parameters for PMSM drives via a network of interconnected extended sliding-mode observers," *IEEE Trans. Power Electron.*, vol. 36, no. 10, pp. 11818–11834, Oct. 2021.

[6] H.-W. Kim, H.-J. Kim, and J.-Y. Choi, "Multiparameter identification for SPMSMs using NLMS adaptive filters and extended sliding-mode observer," *IET Electr. Power Appl.*, vol. 14, no. 4, pp. 533–543, Apr. 2020.

[7] W. Lu, B. Tang, K. Ji, K. Lu, D. Wang, and Z. Yu, "A new load adaptive identification method based on an improved sliding mode observer for PMSM position servo system," *IEEE Trans. Power Electron.*, vol. 36, no. 3, pp. 3211–3223, Mar. 2021.

[8] X. Zhang, J. Zhao, L. Wang, and D. Hu, "High precision anti-interference online multiparameter estimation of PMSLM with adaptive interconnected extend Kalman observer," in *Proc. CSEE*, 2020, pp. 1–10.

[9] K. Kyslan, V. Šlapák, V. Fedák, F. Ďurovský, and K. Horváth, "Design of load torque and mechanical speed estimator of PMSM with unscented Kalman filter—An engineering guide," in *Proc. 19th Int. Conf. Elect. Drives Power Electron.*, 2017, pp. 297–302.

[10] X. Li and R. Kennel, "General formulation of Kalman-filter-based online parameter identification methods for VSI-fed PMSM," *IEEE Trans. Ind. Electron.*, vol. 68, no. 4, pp. 2856–2864, Apr. 2021.
[11] O. C. Kivanc and S. B. Ozturk, "Sensorless PMSM drive based on stator feedforward voltage estimation improved with MRAS multiparameter estimation," *IEEE/ASME Trans. Mechatronics*, vol. 23, no. 3, pp. 1326–1337, Jun. 2018.
[12] H. Zhao *et al.*, "Parameter identification based online noninvasive estimation of rotor temperature in induction motors," *IEEE Trans. Ind. Appl.*, vol. 57, no. 1, pp. 417–426, Jan./Feb. 2021.
[13] R. Garrido and A. Concha, "Inertia and friction estimation of a velocity-controlled servo using position measurements," *IEEE Trans. Ind. Electron.*, vol. 61, no. 9, pp. 4759–4770, Sep. 2014.
[14] A. R. Nair, R. Bhattarai, M. Smith, and S. Kamalasadan, "Parametrically robust identification based sensorless control approach for doubly fed induction generator," *IEEE Trans. Ind. Appl.*, vol. 57, no. 1, pp. 1024–1034, Jan./Feb. 2021.
[15] K. Liu and Z. Zhu, "Fast determination of moment of inertia of permanent magnet synchronous machine drives for design of speed loop regulator," *IEEE Trans. Control Syst. Technol.,* vol. 25, no. 5, pp. 1816–1824, Sep. 2017.
[16] L. Jinhai, C. Wei, and H. Jingao, "Novel experimental methods of acquiring dq inductance of permanent magnet synchronous motors," *Trans. China Electrotech. Soc.*, vol. 29, no. 7, pp. 98–103, Jul. 2014.
[17] S. A. Odhano, R. Bojoi, Ş. G. Roşu, and A. Tenconi, "Identification of the magnetic model of permanent-magnet synchronous machines using DC-biased low-frequency AC signal injection," *IEEE Trans. Ind. Appl.*, vol. 51, no. 4, pp. 3208–3215, Jul./Aug. 2015.
[18] G. Wang *et al.*, "Self-commissioning of permanent magnet synchronous machine drives at standstill considering inverter nonlinearities," *IEEE Trans. Power Electron.*, vol. 29, no. 12, pp. 6615–6627, Dec. 2014.
[19] Y. Shi, K. Sun, L. Huang, and Y. Li, "Online identification of permanent magnet flux based on extended Kalman filter for IPMSM drive with position sensorless control," *IEEE Trans. Ind. Electron.*, vol. 59, no. 11, pp. 4169–4178, Nov. 2012.
[20] B. Aubert, J. Regnier, S. Caux, and D. Alejo, "Kalman-filter-based indicator for online interturn short circuits detection in permanent-magnet synchronous generators," *IEEE Trans. Ind. Electron.*, vol. 62, no. 3, pp. 1921–1930, Mar. 2015.
[21] T. Senjyu, Y. Kuwae, N. Urasaki, and K. Uezato, "Accurate parameter measurement for high speed permanent magnet synchronous motors," in *Proc. IEEE 32nd Annu. Power Electron. Specialists Conf.*, 2001, vol. 2, pp. 772–777.
[22] A. Khlaief, M. Boussak, and A. Châari, "A MRAS-based stator resistance and speed estimation for sensorless vector controlled IPMSM drive," *Electr. Power Syst. Res.*, vol. 108, no. 3, pp. 1–15, 2014.
[23] W. Deng, C. Xia, Y. Yan, Q. Geng, and T. Shi, "Online multiparameter identification of surface-mounted PMSM considering inverter disturbance voltage," *IEEE Trans. Energy Convers.*, vol. 32, no. 1, pp. 202–212, Mar. 2017.
[24] F. Mendoza-Mondragón, V. M. Hernández-Guzmán, and J. Rodríguez-Reséndiz, "Robust speed control of permanent magnet synchronous motors using two-degrees-of-freedom control," *IEEE Trans. Ind. Electron.*, vol. 65, no. 8, pp. 6099–6108, Aug. 2018.
[25] W. Tang, J. Huang, J. Wu, and Q.-G. Wang, "A PID tuning method based on dominant poles and phase margin," in *Proc. 29th Chin. Control Conf.*, 2010, pp. 3402–3405.
[26] K. Li, "PID tuning for optimal closed-loop performance with specified gain and phase margins," *IEEE Trans. Control Syst. Technol.,* vol. 21, no. 3, pp. 1024–1030, May 2013.
[27] W. Lina, Z. Hongyue, and Y. Zongjun, "Tuning method for PI controllers of PMSM driving system," *Trans. China Electrotech. Soc.*, vol. 29, no. 5, pp. 104–117, May 2014.
[28] P. Kshirsagar *et al.*, "Implementation and sensorless vector-control design and tuning strategy for SMPM machines in fan-type applications," *IEEE Trans. Ind. Appl.,* vol. 48, no. 6, pp. 2402–2413, Nov./Dec. 2012.
[29] P. Cui, D. Zhang, S. Yang, and H. Li, "Friction compensation based on time-delay control and internal model control for a gimbal system in magnetically suspended CMG," *IEEE Trans. Ind. Electron.*, vol. 64, no. 5, pp. 3798–3807, May 2017.
[30] X.-C. Jiang and X.-F. Peng, "Two-degree-freedom internal model control for current loop of small rotational inertia PMSM," *Electr. Mach. Control*, vol. 15, no. 8, pp. 69–74, Aug. 2011.
[31] X. Z. Huang *et al.*, "Detent-force minimization of double-sided permanent magnet linear synchronous motor by shifting one of the primary components," *IEEE Trans. Ind. Electron.*, vol. 67, no. 1, pp. 180–191, Jan. 2020.

Yiwei Zhang received the B.E. degree in electrical engineering in 2020 from the Nanjing University of Aeronautics and Astronautics, Nanjing, China, where he is currently working toward the Ph.D. degree in power electronics and electrical drives.

His main research interests include parameter identification technique and permanent magnet synchronous motor control strategy.

Xuzhen Huang (Member, IEEE) received the B.E., M.E., and Ph.D. degrees in electrical engineering from the Harbin Institute of Technology, Harbin, China, in 2006, 2008, and 2012, respectively.

She is currently a Professor with the Department of Electrical Engineering and Automation, Nanjing University of Aeronautics and Astronautics, Nanjing, China. Her current research interests include linear motor system, permanent magnet synchronous motor system, and thermal analysis of motors.

Anpeng Wang was born in Jiangsu, China. He received the B.S. degree in electrical and automation engineering from Nanjing Normal University, Nanjing, China, and the M.S. degree in electrical engineering from the Nanjing University of Aeronautics and Astronautics, Nanjing, China, in 2018 and 2021, respectively. He is currently working toward the Ph.D. degree in electrical engineering with the School of Electrical Engineering, Harbin Institute of Technology, Harbin, China.

His main research interests include linear motor control and predictive control.

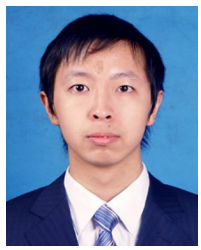

Jian Xu received the B.E. and M.E. degrees in mechatronics engineering from the Harbin Institute of Technology, Harbin, China, in 2006 and 2008, respectively.

He is currently a Research Faculty Member, working with Wuxi Research Institute, Nanjing University of Aeronautics and Astronautics, Nanjing, China. His current research interests include linear motor driver and control system, and mechatronics control system.